# Lawrence Berkeley National Laboratory

**Title**
Formation of metallic copper nanoparticles at the soil-root interface

**Permalink**
https://escholarship.org/uc/item/5zt9c7j6

**Journal**
Environmental Science and Technology, 42(5)

**Authors**
Manceau, Alain
Nagy, Kathryn L.
Marcus, Matthew A.
et al.

**Publication Date**
2008-06-23

# Formation of Metallic Copper Nanoparticles at the Soil–Root Interface

ALAIN MANCEAU,*,† KATHRYN L. NAGY,‡
MATTHEW A. MARCUS,§
MARTINE LANSON,†
NICOLAS GEOFFROY,†
THIERRY JACQUET,△ AND
TATIANA KIRPICHTCHIKOVA△

*LGIT-Maison des Géosciences, CNRS and Université J.
Fourier, 38041 Grenoble Cedex 9, France, Department of Earth
and Environmental Sciences, 845 West Taylor Street, MC-186,
University of Illinois at Chicago, Chicago, Illinois 60607,
Advanced Light Source, Lawrence Berkeley National
Laboratory, One Cyclotron Road, Berkeley, California 94720,
and Phytorestore—Site et Concept, Hôtel Vigée Le Brun,
8 rue du Sentier, 75002 Paris, France*

Copper is an essential element in the cellular electron-transport chain, but as a free ion it can catalyze production of damaging radicals. Thus, all life forms attempt to prevent copper toxicity. Plants diminish excess copper in two structural regions: rare hyperaccumulators bind cationic copper to organic ligands in subaerial tissues, whereas widespread metal-tolerant plants segregate copper dominantly in roots by mechanisms thought to be analogous. Here we show using synchrotron microanalyses that common wetlands plants *Phragmites australis* and *Iris pseudoacorus* can transform copper into metallic nanoparticles in and near roots with evidence of assistance by endomycorrhizal fungi when grown in contaminated soil in the natural environment. Biomolecular responses to oxidative stress, similar to reactions used to abiotically synthesize $Cu^0$ nanostructures of controlled size and shape, likely cause the transformation. This newly identified mode of copper biomineralization by plant roots under copper stress may be common in oxygenated environments.

## Introduction

Copper is toxic to life at levels that vary depending on the organism. Humans are mandated to not exceed 1–2 mg/L copper in their drinking water (1, 2), while some freshwater animals and plants experience acute toxic effects at concentrations as low as 10 $\mu$g/L (3). Because the human food chain begins with plants, it is critical to understand how plants tolerate heavy metals including copper, which is frequently concentrated in soils as a result of pesticide application, sewage sludge deposition, mining, smeltering, and industrial activities. This issue is also at the crux of applying phytoremediation approaches, which use green plants to decontaminate or contain polluted soils and sediments and to purify wastewaters and landfill leachates (4).

Metal-tolerant plants inhibit incorporation of excess metal into photosynthetic tissue by restricting transport across the root endodermis (stele) and by storage in the root cortex (5). In contrast, hyperaccumulating plants extract metals from soils and concentrate excess amounts in harvestable parts such as leaves. Copper detoxification seems to be linked to mechanisms that bind Cu to molecular thiol (SH) groups. Cysteine-rich peptides, such as phytochelatins which transport copper to the shoot, increase in response to high cellular levels of Cu (6, 7), and Cu–S binding occurs in roots and leaves of *Larrea tridentata* (Creosote bush) (8). However, an unidentified copper species, concentrated in electron-dense granules on cell walls and some vacuole membranes, appears to be the main morphological form of copper sequestered in *Oryza sativa* (rice), *Cannabis sativa* (marijuana), *Allium sativum* (garlic), and *Astragalus sinicus* (Chinese milk vetch) (9–12).

Plants take in and exclude elements largely at the soil–root interface within the rhizosphere, i.e. the volume of soil influenced by roots, mycorrhizal fungi, and bacterial communities (13). Deciphering processes that control the bioavailability of metals in the field is difficult because the rhizosphere is compositionally and structurally complex. Here we report on using synchrotron-based microanalytical and imaging tools (14) to resolve processes by which metal-tolerant plants defend themselves against excess cationic copper. We have mapped the distribution of copper in self-standing thin sections of unperturbed soils using micro-X-ray fluorescence ($\mu$-XRF) and identified structural forms of copper at points-of-interest (POIs) using micro-extended X-ray absorption fine structure ($\mu$-EXAFS) spectroscopy and X-ray diffraction ($\mu$-XRD). Because only a few small areas could be analyzed in reasonable times with microanalyses, the uniqueness of the microanalytical results was tested by recording the bulk EXAFS spectrum from a sample representing the entire rhizosphere and by simulating this spectrum by linear combination of copper species spectra from POIs.

We investigated copper speciation in rhizospheres of *Phragmites australis* (common reed) and *Iris pseudoacorus*, two widespread wetland species with high tolerances to heavy metals (15). *P. australis* is frequently used to treat wastewaters (16) because it can store heavy metals as weakly soluble or insoluble forms. Its roots can be enriched in Cu 5–60 times relative to leaves, with large differences among ecotypes and between field-grown versus hydroponically grown plants (17, 18). To take into account natural complexity, including any influence of bacteria, fungi, or climate variation, our experiment was conducted outdoors, rather than in a greenhouse on seedlings using ex-solum pots or hydroponic growth methods. The soil was from the Pierrelaye plain, a 1200 ha truck-farming area about 30 km northwest of Paris, France. From 1899 to 1999, regular irrigation of the Pierrelaye plain with untreated sewage water from Paris caused contamination with heavy metals, mainly Zn, Pb, and Cu (19). Such pollution is pervasive worldwide because increasing populations and associated economic growth are diminishing available freshwater, thus leading to increased irrigation of farmlands with wastewaters.

## Experimental Methods

**Field Experiment.** A detailed description of the phytoremediation experiment is given in Supporting Information.

* Corresponding author e-mail: manceau@obs.ujf-grenoble.fr.
† LGIT-Maison des Géosciences.
‡ University of Illinois at Chicago.
§ Lawrence Berkeley National Laboratory.
△ Phytorestore—Site et Concept.
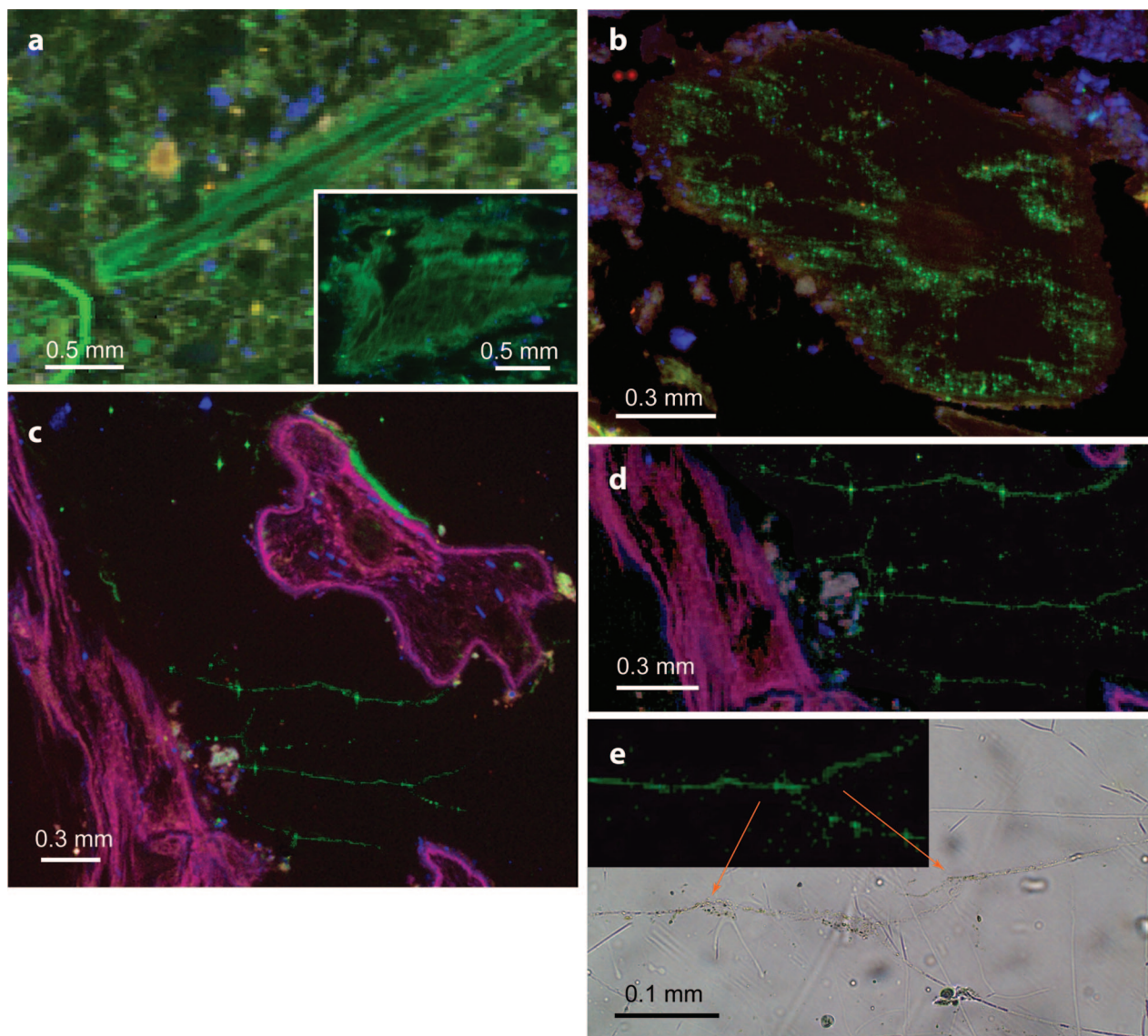
**FIGURE 1.** Micro-X-ray fluorescence ($\mu$-XRF) maps showing the distribution of Zn (red), Cu (green), and Ca (blue) in the initial soil (a) and rhizospheres of *Phragmites australis* (b) and *Iris pseudoacorus* (c–e). (a) Green features are organic matter (resolution = 20 × 20 $\mu$m²). The inset shows a reticular structure mapped at high resolution (9 × 9 $\mu$m²). (b) Transversal section of a root with aggregates of Cu metal nanoparticles in the cortical region (resolution = 4 × 4 $\mu$m²). The central stele region contains Zn but no Cu. (c) Although Zn occurs in the main roots of *I. pseudoacorus*, Cu is located in ramified organic filaments typical of mycorrhizal fungi and in a biofilm at the surface of the root (resolution = 8 × 8 $\mu$m²). (d) Enlargement of the region rich in organic filaments showing two anastomosed hyphae. (e) Optical micrograph of one anastomosed hypha from panel d with fluorescence map in inset. Data collected on beamline 10.3.2 of the Advanced Light Source (ALS) at Lawrence Berkeley National Laboratory (*62*).

**X-ray Fluorescence.** Elemental distributions in the initial soil and rhizospheric soils vegetated with *P. australis* and *I. pseudoacorus* were mapped by scanning several 30-$\mu$m-thick thin sections under a 10.0 keV (vegetated soil) or 13.05 keV (unvegetated soil) micro-X-ray beam while recording the X-ray fluorescence. The soil is rich in organic debris from past agricultural activity which causes it to be optically inhomogeneous over a few to several hundreds of micrometers. Therefore, both coarse and fine $\mu$-XRF maps were recorded at resolutions from 35 × 35 $\mu$m² to 4 × 4 $\mu$m² using a beam dimension adjusted from 16 (H) × 10 (V) $\mu$m² to 5 (H) × 5 (V) $\mu$m² to match the step size. The counting time per pixel was 100 ms at 10.0 keV and 200 ms at 13.05 keV. The scanning speed was fast enough to prevent alteration of the initial Cu speciation by beam damage.

**EXAFS Spectroscopy.** In the $\mu$-EXAFS measurement, the organically bound Cu species evolved over 30–45 min due to the instability of organic matter to intense X-ray radiation. Radiation damage was minimized by reducing scan times to 20 min per analyzed area and moving the sample by 15 $\mu$m along the direction of an organic particle to access fresh material for every scan. Caution was taken that all individual spectra averaged out before summing to improve statistics. For bulk EXAFS measurements, samples were frozen at 10 K. All spectra were recorded in fluorescence-yield detection mode, except those from the Cu grains ($\mu$-EXAFS), which were recorded in transmission mode.

**X-ray Diffraction.** Diffraction patterns were recorded in transmission mode with a Bruker 6000 CCD binned to 1024 × 1024 pixels.

## Results and Interpretations

**X-ray Fluorescence.** In the initial soil, copper occurs in two morphological forms (Figure 1a). One form decorates coarse organic particles that have some recognizable structures from reticular tissue (insert in Figure 1a), and the other occurs in
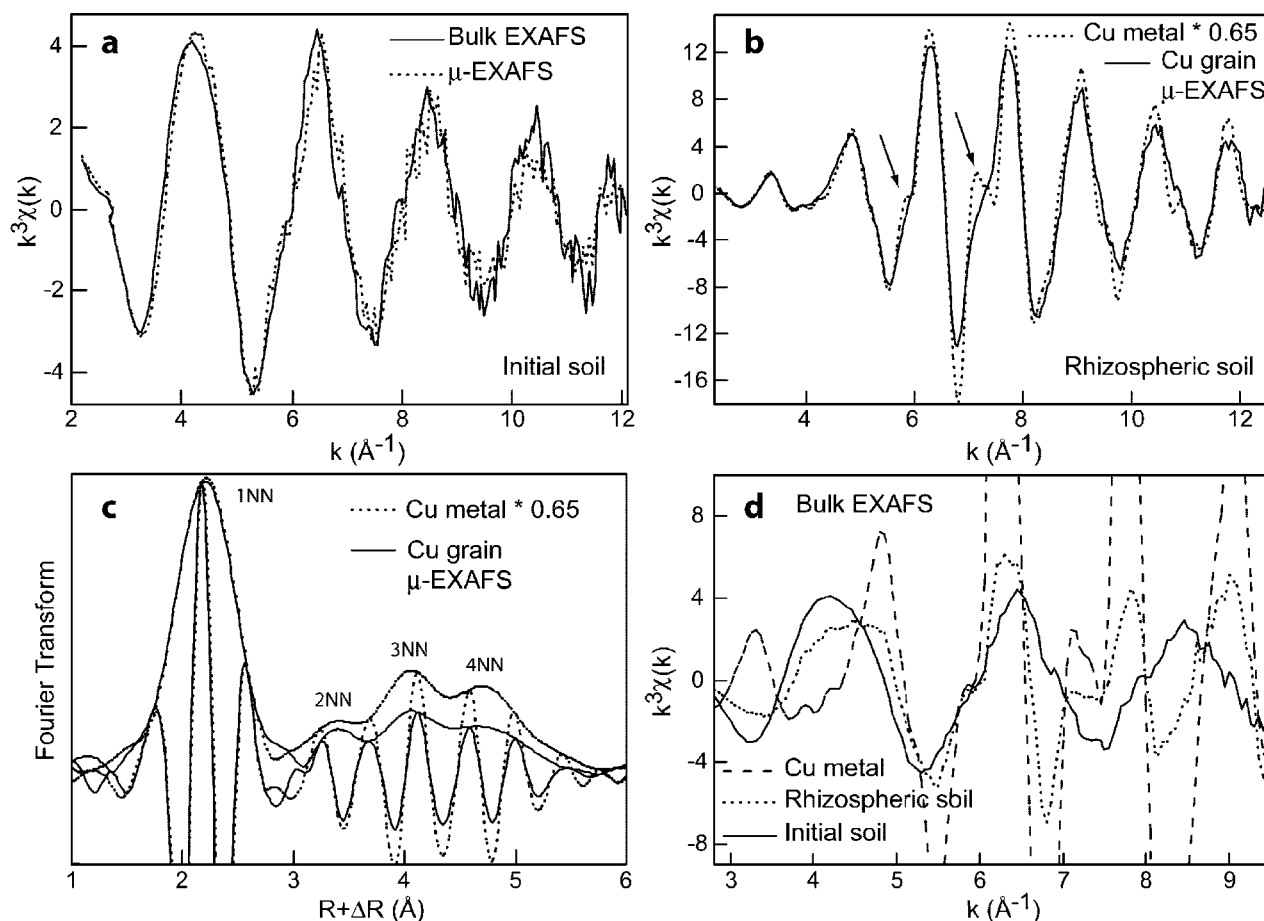
**FIGURE 2. EXAFS data. (a) Representative Cu K-edge $\mu$-EXAFS spectrum at room temperature of organic debris (dotted line) from the map in Figure 1a and the bulk EXAFS spectrum at 10 K of the initial soil (solid line). (b) Representative $\mu$-EXAFS spectrum of Cu grains from *P. australis* rhizosphere (solid line) and bulk EXAFS spectrum of reference Cu metal at room temperature. The amplitude of the reference spectrum was multiplied by 0.65. (c) Fourier transform (modulus plus imaginary part) of the EXAFS spectra in panel b. The amplitude of the reference's first shell peak (1NN contribution) was scaled to that of the sample by multiplying the reference EXAFS signal by 0.65. (d) Bulk EXAFS spectra of the initial soil (10 K, solid line), *P. australis* rhizosphere (10 K, dotted line), and Cu metal (room temperature, dashed line). The spectrum for the *I. pseudoacorus* rhizosphere is similar to that of *P. australis* and was omitted for clarity. The $\mu$-EXAFS data were recorded on beamline 10.3.2 at the ALS and the bulk EXAFS data on the FAME beamline (BM 30B) at the European Synchrotron Radiation Facility (ESRF, France) (63).**

the fine clayey matrix in areas that show organic particulate shapes only at high $\mu$-XRF resolution. In the two phytore-mediated soils, similar Cu−organic particulate associations, but also, hot spots of Cu grains 5−20 $\mu$m in size were observed in the thin-section maps (Figure 1b−d). In the rhizosphere of *P. australis*, the Cu hot spots exist outside and in roots and specifically in cortical parenchyma, but not in central vascular cylinders from the stele that contain vascular bundles through which micronutrients are transported to reproductive and photosynthetic tissues. In contrast, the main roots and rhizome of *I. pseudoacorus* do not contain detectable Cu grains, but in the surrounding soil Cu grains are aligned, suggesting that they are associated with biological structures. Under an optical microscope filamentous and ramified organic structures, similar to root hairs or hyphae from endomycorrhizal fungi, are visible in places where the Cu spots were observed by $\mu$-XRF (Figure 1e, Supporting Information). Fungal forms are more likely because my-corrhizal hyphae typically are anastomosing, whereas root hairs are not. Fungi may also be implicated in the formation of Cu grains in the cortex of *P. australis* since roots of this plant are known to be colonized by arbuscular endomy-corrhizae in contaminated environments (20). These hy-potheses are consistent with the capacity of mycorrhizae to accumulate metals (21–23) and with the storage of Cu in secondary feeder roots of the water hyacinth *Eichhornia*

*crassipes* (24). The Cu grains have about the same size as the electron-dense Cu granules (~2 $\mu$m) in cells of *E. splendens* placed in a $CuSO_4$ solution for 30 days (12).

**EXAFS Spectroscopy.** *Organic Cu.* While biological activity clearly modified the original distribution of Cu in the rhizospheres, the Cu species could not be identified from the $\mu$-XRF maps but instead were elucidated using EXAFS spectroscopy. All eight $\mu$-EXAFS spectra from areas in the original soil containing the particle morphologies and chemical compositions observed with $\mu$-XRF can be super-imposed on the soil's bulk EXAFS spectrum (Figure 2a), indicating that the initial Cu speciation occurred uniformly. If the initial soil contained various assemblages of Cu species that were distributed unevenly, then we might expect that the proportions of species also would have varied among analyzed areas and been detectable by $\mu$-EXAFS spectroscopy (25); however, this was not observed. These spectra match those for $Cu^{2+}$ binding to carboxyl ligands in natural organic matter, as commonly observed (Supporting Information).

*Elemental Cu.* In contrast, only the reference spectrum of elemental copper ($Cu^0$) matches the $\mu$-EXAFS spectra of the 12 hot-spot Cu grains, which are statistically invariant (Figure 2b, Supporting Information). Photoreduction of $Cu^{2+}$ in the X-ray beam cannot explain the formation of $Cu^0$ because (i) no elemental Cu was detected in the initial soil by powder and $\mu$-EXAFS, and (ii) $Cu^0$ was detected in the two phytore-

mediated soils at 10 K by bulk EXAFS, and all individual spectral scans from the same sample could be superimposed. At 10 K, radiation damage is delayed (*14*), and if Cu had been reduced in the beam, the proportion of $Cu^0$ would have increased from scan to scan which was not observed.

Spectra for rhizosphere Cu grains and reference metallic copper have the same phase and overall line shape, but they have significant differences in fine structure and amplitude, which provide details about the nature of the Cu grains. In the soil Cu grains, shoulders at 5.8 and 7.3 $Å^{-1}$ are weak and the spectral amplitude is reduced by about 35% and attenuated, relative to metallic copper. The decreased amplitude of the EXAFS signal for the Cu grains relative to well-crystallized metallic copper cannot arise from overabsorption (*14*) because the spectra of the grains were recorded in transmission mode and because the amplitude reduction from overabsorption would be uniform in *R*-space, as demonstrated for ZnS and $MnO_2$ particles (*26, 27*), which does not occur in this case.

Derived radial structure–functions share the four-peak character of Cu metal (*28*) (Figure 2c). However, long-distance pair correlations (i.e., the high-frequency components in *k* space) are progressively diminished in the soil spectra, indicating multiple interatomic distances (structural disorder), reduced coordination numbers (CNs) from small particles (size effect), and/or abundant microstructural defects, such as grain and twin boundary dislocations or atomic-scale vacancies.

Simulation of the data using multiple-scattering ab initio FEFF calculations showed no evidence for structural disorder (Supporting Information). Good agreement between calculated and observed spectra was obtained with a first nearest-neighbor shell (1NN) of 7.8 Cu atoms at 2.55 Å, a second shell (2NN) of 2.7 Cu at 3.61 Å, a third shell (3NN) of 9.2 Cu at 4.43 Å, and a fourth shell (4NN) of 3.9 Cu at 5.11 Å, compared to 1NN of 12 at 2.55 Å, 2NN of 6 at 3.61 Å, 3NN of 24 at 4.43 Å, and 4NN of 12 at 5.11 Å, in crystalline Cu metal. The mean-square displacement of bond length parameter ($\sigma^2$), a measure of disorder, converged in the simulated spectra to the same value as in the Cu metal reference (0.01 $Å^2$) showing that Cu–Cu bonds vary in length by the same amount in the soil grains and reference.

Although the rhizosphere Cu grains are not structurally disordered, their CNs are only 65% (1NN), 45% (2NN), 38% (3NN), and 32% (4NN) of those in the Cu metal spectrum, indicating that structural order is limited in extent. The lower CN values are consistent with small particles having incompletely coordinated surface atoms. If closed-shell packed and monodispersed, these particles would have a minimum size of 10–15 Å assuming a spherical cuboctahedron shape and 15–20 Å assuming a hemispherical shape, as reported for nanoscale platinum particles (*29*). If Cu atoms were missing (e.g., atomic vacancies), as reported for Fe metal powders with a first-shell CN reduced by up to 50% of that in metallic Fe, the effective particle size could be as high as ca. 100 Å in diameter (*30*). A defective nanoparticle model is appealing because the surface area-to-volume ratio increases with only a lattice-vacancy parameter.

Constitutive nanoparticles in the micrometer-sized Cu grains are joined at particle or so-called grain boundaries, which might contain stabilizing organic molecules. Complexation of Cu to sulfur ligands in the interparticle or surficial regions is unlikely because a low-*R* Fourier component from Cu–S pairs at 2.2–2.3 Å was not observed on the radial structure–function (*8*). Also, the first Cu–Cu distance of 2.56 Å in the Cu nanoparticle is shorter than the distance of 2.70–2.90 Å reported for Cu–thiolate clusters (*8, 31*) and matches only that in elemental copper. In addition, organic S or P was not observed in the Cu grains using scanning electron microscopy–energy dispersive X-ray fluorescence

(SEM-EDX) in agreement with observations on electron-dense Cu granules in plants using electron energy loss spectroscopy (EELS) and EDX (*10, 12*). Complexation to oxygen ligands is possible because EXAFS has relatively low sensitivity to low-Z atoms. However, linear combinations of experimental spectra for organically bound $Cu^{2+}$ and nanometallic Cu show that the fraction of potential organic Cu in the Cu grains is less than 15%, if present at all (Supporting Information).

*Amounts of Organic and Elemental Cu in the Rhizospheres.* Composite bulk EXAFS spectra of the two remediated soils and spectra from the two species identified by $\mu$-EXAFS (Figure 2d) intersect at the same *k* values, confirming that only two main Cu species exist in both rhizospheres. Fractional amounts of organically bound Cu from the original soil and metallic Cu formed during phytoremediation were estimated by reconstructing the bulk spectra with linear combinations of the two single species spectra. The best fit for the rhizosphere of *P. australis* was obtained with 75 ± 10% organic-bound $Cu^{2+}$ and 25 ± 10% $Cu^0$. The rhizosphere of *I. pseudoacorus* contains slightly less $Cu^0$ (20 ± 10%).

**X-ray Diffraction.** Featureless two-dimensional $\mu$-XRD patterns from eight Cu hot spots confirm that the Cu grains are aggregates of nanoparticles. However, three patterns display a faint continuous diffraction ring at the Bragg angle for the brightest 111 reflection of Cu metal, indicating larger individual particles with a domain size of 130–150 Å (Figure 3). About $25 \times 10^4$ larger particles would be needed to produce these XRD patterns, but they would comprise only about 0.01% of the analyzed volume (Supporting Information). Thus, the diffracting Cu hot spots may have sufficient big particles to yield a powder ring, but they are not enough for their 2NN, 3NN, and higher Cu-Cu shells to contribute significantly to the EXAFS signal. Also, the big particles are undetected by $\mu$-EXAFS because EXAFS signal intensity is linearly proportional to the number of atoms whereas XRD intensity is proportional to the number of atoms squared.

## Discussion

**Mechanism of $Cu^{2+}$ to $Cu^0$ Reduction.** The rhizospheres were oxidizing as indicated by the presence of iron oxyhydroxide (goethite), absence of sulfide minerals, and the fact that *P. australis* and *I. pseudoacorus* are typical wetlands plants with aerenchyma that facilitate oxygen flow from leaves to roots (*32*). Thermodynamic calculations using compositions of soil solutions collected below the rhizosphere indicate that $Cu^+$ and $Cu^{2+}$ species should have been dominant (Supporting Information). These points along with the occurrences of nanocrystalline $Cu^0$ in plant cortical cells and as stringer morphologies outside the roots together suggest that copper was reduced biotically. Ecosystem ecology of the rhizosphere indicates synergistic or multiple reactions by three types of organisms: plants, endomycorrhizal fungi, and bacteria.

Normally, organisms maintain copper homeostasis through cation binding to bioactive molecules such as proteins and peptides. When bound, the $Cu^{2+}/Cu^{1+}$ redox couple has elevated half-cell potentials (*33*) that facilitate reactions in the electron-transport chain. Even though average healthy cell environments are sufficiently reducing (*34*), there are enough binding sites (*35*) to maintain copper in its two oxidized states. Copper is also important in controlling cell-damaging free radicals produced at the end of the electron-transport chain, for example in the superoxide dismutase enzyme Cu-Zn-SOD, which accelerates the disproportionation of superoxide to $O_2$ and hydrogen peroxide. However, unbound copper ions can catalyze the decomposition of hydrogen peroxide to water and more free radical species. To combat toxic copper and free radicals, many organisms overproduce enzymes such as catalase, chelates such as glutathione, and antioxidants (*36*). Mineralization

FIGURE 3. XRD data. (a) Two-dimensional $\mu$-XRD pattern of a Cu grain showing the 111, 200, and 220 reflections of Cu metal. The spotty reflections are from coarse quartz grains ($d$ = 2.28, 2.24, 1.82, 1.66 Å), and were used as internal calibration standards. (b) One-dimensional patterns obtained by summing intensities radially at constant Bragg angle. The pattern in black is from the Cu grain whose 2D pattern is shown in panel a. The two other patterns are from different grains. Their 111 reflections are too faint to be viewed on the 2D image, and they can be observed only after integration. The $d$(111) and $d$(200) spacings are shifted by +0.015 to +0.04 Å relative to pure $Cu^0$ ($d$(111) = 2.09 Å and $d$(200) = 1.81 Å), due probably to the incorporation of trace elements (e.g., Sn, W, Zn), as commonly observed in metallic copper. Recording conditions: energy = 17 keV, beam size = 16 (H) × 7 (V) $\mu m^2$, exposure time = 120 s.

could also be a defense against toxic copper, but reports of $Cu^+$ and $Cu^{2+}$ biominerals are rare; only copper sulfide in yeast (37) and copper oxalate in lichens (38) and fungi (23) are known. Atacamite ($Cu_2(OH)_3Cl$) in worms (39) does not appear to result from a biochemical defense.

Biomineralization of copper metal may have occurred by a mechanism analogous to processes for metallic nanoparticle synthesis that exploit ligand properties of organic molecules. In these processes, organic molecules are used as templates to control the shape and size of metallic nanoparticles (40, 41) formed by adding strong reductants to bound cations. For copper nanoparticles and nanowires, a milder reductant—ascorbic acid—has been used. Ascorbic acid, a well-known antioxidant, reduces Cu cations to $Cu^0$ only when the cations are bound to organic substrates such as DNA in the presence of oxygen in the dark (42) or via autocatalysis on Cu metal seeds in the absence of stabilizing organic ligands (43). As an example of synthetic control, pH-dependent conformation of histidine-rich peptides has led to larger nanocrystals of $Cu^0$ at pH 7–10 than at pH 4–6 (44).

Plants produce ascorbic acid for many functions (45) and rhizospheres often contain the breakdown products of ascorbic acid, which facilitates electron transfer during mineral weathering (46). Plants produce more ascorbic acid when grown in soils contaminated with heavy metals including copper (47). Fungi, which proliferate over plants (48) and bacteria (23) in metal-contaminated soils, can stabilize excess copper (49) by extracellular cation binding or oxalate precipitation (23), but mechanisms probably also require enzymes, thiol-rich proteins and peptides, and antioxidants (23, 48, 50). The formation of electron-dense Cu granules within hyphae of arbuscular mycorrhizal fungi isolated from Cu- and As-contaminated soil (51) suggests that fungi also can produce nanoparticulate copper.

Some copper reduction possibly occurred in response to the European heat wave of the summer of 2003 (Supporting Information). Elevated expression of heat shock protein HSP90 and metallothionein genes has been observed in hyphae of an arbuscular mycorrhizal fungus in the presence of $2 \times 10^{-5}$ M $CuSO_4$ in the laboratory (52). This suggests that a single driving force can trigger a biological defense mechanism that has multiple purposes. Thus, reduction of toxic cations to native elements may increase as rhizosphere biota fight metal stress and stresses imposed by elevated temperatures expected from global warming.

**Reduction of Other Metal Cations to Their Metallic Forms.** Laboratory evidence has shown that plants (53–55), fungi (23, 56, 57), bacteria (58), and algae (59) can transform other more easily reducible metals, including Au, Ag, Se (as $H_2SeO_3$), Hg, and Te, to their elemental states both intra- and extracellularly. When mechanisms have been proposed, they typically have involved enzymes; however, ascorbic acid was implicated when $Hg^{2+}$ was transformed to $Hg^0$(g) in barley leaves (60). Theoretically all of these metal cations could be transformed by a reducing agent weaker than ascorbic acid (Table S1 in Supporting Information). However, binding appears to stabilize cationic forms in the absence of a sufficiently strong reductant such as ascorbic acid. Processes used in materials synthesis that were developed with biochemical knowledge might yield clues to other possible, but presently unknown, biologically mediated reactions in different organisms.

**Natural Occurrence of $Cu^0$ and Environmental Implications.** The discovery of nanoparticulate copper metal in phytoremediated soil may shed light on the occurrence of copper in peats. Native copper likely forms abiotically in the reducing acidic environments of Cu-rich peat bogs (61). However, swamps by definition are more oxidizing with neutral to alkaline pHs, and they may be ideal sites for biotic formation of metallic Cu nanoparticles. For example, in swamp peats near Sackville, New Brunswick, Canada, copper species unidentifiable by XRD were dissolved only with corrosive perchloric acid (61), suggesting they may have been nanoparticulate metal formed by active root systems of swamp plants. If swamp peats evolve to bog peats the Cu reduction mechanism could convert to autocatalysis on the

initial nanocrystals (*43*). The addition of peats that either act as templating substrates or contain nanoparticulate copper could enhance the effectiveness of using wetlands plants for phytoremediation. In contrast to harvesting hyperaccumulators, the oxygenated rhizosphere would become an economic source of biorecycled copper, and rhizosphere containment would prevent copper from entering the food chain via herbivores, limiting potential risks to humans.

## Supporting Information Available

Additional information on the field site, and data interpretations, including thermodynamic calculations of Cu speciation in the soil solution. This material is available free of charge via the Internet at http://pubs.acs.org.

## Literature Cited

(1) OJEC. On the quality of water intended for human consumption. *Off. J. Eur. Communities* **1998**, *L-330* (5 December 1998).

(2) EPA National primary drinking water standards. EPA Agency, 2003, EPA-816-F-03-016.

(3) EPA Aquatic life ambient freshwater quality criteria - copper 2007 revision. EPA Agency, EPA-822-F07-001.

(4) Vassilev, A.; Schwitzguébel, J. P.; Thewys, T.; Van der Lelie, D.; Vangronsveld, J. The use of plants for remediation of metal-contaminated soils. *Sci. World J.* **2004**, *4*, 9–34.

(5) MacFarlane, G. R.; Burchett, M. D. Cellular distribution of copper, lead and zinc in the grey mangrove, *Avicennia marina* (Forsk.) Vierh. *Aquat. Bot.* **2000**, *68*, 45–59.

(6) Van Hoof, N. A. L. M.; Hassinen, V. H.; Hakvoort, H. W. J.; Ballintijn, K. F.; Schat, H.; Verkleij, J. A. C.; Ernst, W. H. O.; Karenlampi, S. O.; Tervahauta, A. I. Enhanced copper tolerance in *Silene vulgaris* (Moench) Garcke populations from copper mines is associated with increased transcript levels of a 2b-type metallothionein gene. *Plant Physiol.* **2001**, *126*, 1519–1526.

(7) Clemens, S. Molecular mechanisms of plant metal tolerance and homeostasis. *Planta* **2001**, *212*, 475–486.

(8) Polette, L. A.; Gardea-Torresdey, J. L.; Chianelli, R. R.; George, G. N.; Pickering, I. J.; Arenas, J. XAS and microscopy studies of the uptake and bio-transformation of copper in *Larrea tridentate* (creosote bush). *Microchem. J.* **1998**, *65*, 227–236.

(9) Lidon, F. C.; Henriques, F. S. Subcellular localization of copper and partial isolation of copper proteins in roots from rice plants exposed to excess copper. *Aust. J. Plant Physiol.* **1994**, *21*, 427–436.

(10) Arru, L.; Rognoni, S.; Baroncini, M.; Bonatti, P. M.; Perata, P. Copper localization in *Cannabis sativa* L. grown in a copper-rich solution. *Euphytica* **2004**, *140*, 33–38.

(11) Liu, D.; Kottke, I. Subcellular localization of copper in the root cells of *Allium sativum* by electron energy loss spectroscopy (EELS). *Biores. Technol.* **2004**, *94*, 153–158.

(12) Ni, C. Y.; Chen, Y. X.; Lin, Q.; Tian, G. M. Subcellular localization of copper in tolerant and non-tolerant plant. *J. Environ. Sci. China* **2005**, *17*, 452–456.

(13) Hinsinger, P.; Gobran, G. R.; Gregory, P. J.; Wenzel, W. W. Rhizosphere geometry and heterogeneity arising from root-mediated physical and chemical processes. *New Phytol.* **2005**, *168*, 293–303.

(14) Manceau, A.; Marcus, M. A.; Tamura, N. Quantitative speciation of heavy metals in soils and sediments by synchrotron X-ray techniques. In *Applications of Synchrotron Radiation in Low-Temperature Geochemistry and Environmental Science*; Fenter, P. A., Rivers, M. L., Sturchio, N. C., Sutton, S. R., Eds.; Mineral. Soc. Amer.: Washington, DC, 2002; Vol. 49, pp 341–428.

(15) Weis, J. S.; Weis, P. Metal uptake, transport and release by wetland plants: Implications for phytoremediation and restoration. *Environ. Intern.* **2004**, *30*, 685–700.

(16) Peverly, J. H.; Surface, J. M.; Wang, T. Growth and trace metal absorption by *Phragmites australis* in wetlands constructed for landfill leachate treatment. *Ecol. Eng.* **1995**, *5*, 21–35.

(17) Stoltz, E.; Greger, M. Accumulation properties of As, Cd, Cu, Pb and Zn by four wetland plant species growing on submerged mine tailings. *Environ. Exp. Bot.* **2002**, *47*, 271–280.

(18) Deng, H.; Ye, Z. H.; Wong, M. H. Accumulation of lead, zinc, copper and cadmium by 12 wetland plant species thriving in metal-contaminated sites in China. *Environ. Pollut.* **2004**, *132*, 29–40.

(19) Kirpichtchikova, T.; Manceau, A.; Spadini, L.; Panfili, F.; Marcus, M. A.; Jacquet, T. Speciation and solubility of heavy metals in contaminated soil using X-ray microfluorescence, EXAFS spectroscopy, chemical extraction, and thermodynamic modelling. *Geochim. Cosmochim. Acta* **2006**, *70*, 2163–2190.

(20) Oliveira, R. S.; Dodd, J. C.; Castro, P. M. L. The mycorrhizal status of *Phragmites australis* in several polluted soils and sediments of an industrialised region of Northern Portugal. *Mycorrhiza* **2001**, *10*, 241–247.

(21) Leyval, C.; Turnau, K.; Haselwandter, K. Effect of heavy metal pollution on mycorrhizal colonization and function: physiological, ecological and applied aspects. *Mycorrhiza* **1997**, *7*, 139–153.

(22) Tonin, C.; Vandenkoornhuyse, P.; Joner, E. J.; Straczek, J.; Leyval, C. Assessment of arbuscular mycorrhizal fungi diversity in the rhizosphere of *Viola calaminaria* and effect of these fungi on heavy metal uptake by clover. *Mycorrhiza* **2001**, *10*, 161–168.

(23) Gadd, G. M. Geomycology: biogeochemical transformations of rocks, minerals, metals and radionuclides by fungi, bioweathering and bioremediation. *Mycol. Res.* **2007**, *111*, 3–49.

(24) Vesk, P. A.; Nockolds, C. E.; Allaway, W. G. Metal localization in water hyacinth roots from an urban wetland. *Plant, Cell Environ.* **1999**, *22*, 149–158.

(25) Panfili, F.; Manceau, A.; Sarret, G.; Spadini, L.; Kirpichtchikova, T.; Bert, V.; Laboudigue, A.; Marcus, M. A.; Ahamdach, N.; Libert, M. F. The effect of phytostabilization on Zn speciation in a dredged contaminated sediment using scanning electron microscopy, X-ray fluorescence, EXAFS spectroscopy and principal components analysis. *Geochim. Cosmochim. Acta* **2005**, *69*, 2265–2284.

(26) Manceau, A.; Marcus, M. A.; Tamura, N.; Proux, O.; Geoffroy, N.; Lanson, B. Natural speciation of Zn at the micrometer scale in a clayey soil using X-ray fluorescence, absorption, and diffraction. *Geochim. Cosmochim. Acta* **2004**, *68*, 2467–2483.

(27) Manceau, A.; Tommaseo, C.; Rihs, S.; Geoffroy, N.; Chateigner, D.; Schlegel, M.; Tisserand, D.; Marcus, M. A.; Tamura, N.; Chen, Z. S. Natural speciation of Mn, Ni and Zn at the micrometer scale in a clayey paddy soil using X-ray fluorescence, absorption, and diffraction. *Geochim. Cosmochim. Acta* **2005**, *69*, 4007–4034.

(28) Zabinsky, S. I.; Rehr, J. J.; Ankudinov, A.; Albers, R. C.; Eller, M. J. Multiple scattering calculations of X-ray absorption spectra. *Phys. Rev.* **1995**, *B52*, 2995–3009.

(29) Frenkel, A. I.; Hills, C. W.; Nuzzo, R. G. A view from the inside: Complexity in the atomic scale ordering of supported metal nanoparticles. *J. Phys. Chem.* **2001**, *105*, 12689–12703.

(30) DiCicco, A.; Berrettoni, M.; Stizza, S.; Bonetti, E.; Cocco, G. Microstructural defects in nanocrystalline iron probed by X-ray absorption spectroscopy. *Phys. Rev.* **1994**, *B50*, 12386–12397.

(31) Heaton, D. N.; George, G. N.; Garrison, G.; Winge, D. R. The mitochondrial copper metallochaperone cox17 exists as an oligomeric, polycopper complex. *Biochemistry* **2001**, *40*, 743–751.

(32) Otte, M. L.; Matthews, D. J.; Jacob, D. L.; Moran, B. M.; Baker, A. J. M. Biogeochemistry of metals in the rhizosphere of wetland plants. An explanation for 'innate' metal tolerance. In *Developments in Ecosystems*; Wong, M. H., Ed.; Elsevier: 2004.

(33) Battistuzzi, G.; Borsari, M.; Canters, G. W.; Loschi, L.; Righi, F.; Sola, M. Redox thermodynamics of blue copper proteins. *J. Am. Chem. Soc.* **1999**, *121*, 501–506.

(34) Schafer, F. Q.; Buettner, G. R. Redox environment of the cell as viewed through the redox state of the glutathione disulfide/glutathione couple. *Free Radical Biol. Med.* **2001**, *30*, 1191–1212.

(35) Huffman, D. L.; O'Halloran, T. V. Function, structure, and mechanism of intracellular copper trafficking proteins. *Annu. Rev. Biochem.* **2001**, *70*, 677–701.

(36) Buettner, G. R.; Jurkiewicz, B. A. Catalytic metals, ascorbate and free radicals: Combinations to avoid. *Radiat. Res.* **1996**, *145*, 532–541.

(37) Gadd, G. M. Interactions of fungi with toxic metals. *New Phytol.* **1993**, *124*, 25–60.

(38) Chisholm, J. E.; Jones, G. C.; Purvis, O. W. Hydrated copper oxalate, moolooite, in lichens. *Miner. Mag.* **1987**, *51*, 715–718.

(39) Lichtenegger, H. C.; Schoberl, T.; Bartl, M. H.; Waite, H.; Stucky, G. D. High abrasion resistance with sparse mineralization: copper biomineral in worm jaws. *Science* **2002**, *298*, 389–392.

(40) Slocik, J. M.; Wright, D. W. Biomimetic mineralization of noble metal nanoclusters. *Biomacromolecules* **2003**, *4*, 1135–1141.

(41) Song, J.; Zhao, F. J.; Luo, Y. M.; McGrath, S. P.; Zhang, H. Z. Copper uptake by *Elsholtzia spendens* and *Silene vulgaris* and assessment of copper phytoavailability in contaminated soils. *Environ. Pollut.* **2004**, *128*, 307–315.

(42) Monson, C. F.; Woolley, A. T. DNA-templated construction of copper nanowires. *Nano Lett.* **2003**, *3*, 359–363.

(43) Jana, N. R.; Wang, Z. L.; Sau, T. K.; Pal, T. Seed-mediated growth method to prepare cubic copper nanoparticles. *Curr. Sci.* **2000**, *79*, 1367–1370.

(44) Banerjee, I. A.; Yu, L.; Matsui, H. Cu nanocrystal growth on peptide nanotubes by biomineralization: Size control of Cu nanocrystals by tuning peptide conformation. *Proc. Natl. Acad. Sci.* **2003**, *1000*, 14678–14682.

(45) Horemans, N.; Foyer, C. H.; Potters, G.; Asard, H. Ascorbate function and associated transport systems in plants. *Plant Physiol. Biochem.* **2000**, *38*, 531–540.

(46) Hering, J. G.; Stumm, W. Oxidative and reductive dissolution of minerals. In *Mineral-Water Interface Geochemistry*; Hochella, M. F. J., White, A. F., Eds.; Mineral. Soc. Am.: 1990; Vol. 23, pp 427–465.

(47) Singh, S.; Saxena, R.; Pandey, K.; Bhatt, K.; Sinha, S. 2004 Response of antioxidants in sunflower (*Helianthus annuus* L.) grown on different amendments of tannery sludge: its metal accumulation potential. *Chemosphere* **2004**, *57*, 1663–1673.

(48) Meharg, A. A. The mechanistic basis of interactions between mycorrhizal associations and toxic metal cations. *Mycol. Res.* **2003**, *107*, 1253–1265.

(49) Bradley, R.; Burt, A. J.; Read, D. J. Mycorrhizal infection and resistance to heavy metal toxicity in *Calluna vulgaris*. *Nature* **1981**, *292*, 335–337.

(50) Schützendübel, A.; Polle, A. Plant responses to abiotic stresses: heavy metal-induced oxidative stress and protection by mycorrhization. *J. Exp. Bot.* **2002**, *53*, 1351–1365.

(51) Gonzalez-Chavez, C.; D'Haen, J.; Vangronsveld, J.; Dodd, J. C. Copper sorption and accumulation by the extraradical mycelium of different *Glomus spp.* (arbuscular mycorrhizal fungi) isolated from the same polluted soil. *Plant Soil* **2002**, *240*, 287–297.

(52) Hildebrandt, U.; Regvar, M.; Bothe, H. Arbuscular mycorrhiza and heavy metal tolerance. *Phytochemistry* **2007**, *68*, 139–146.

(53) Gardea-Torresdey, J. L.; Tiemann, K. J.; Parsons, J. G.; Gamez, G.; Herrera, I.; Jose-Yacaman, M. XAS investigations into the mechanism(s) of Au(III) binding and reduction by alfalfa biomass. *Microchem. J.* **2002**, *71*, 193–204.

(54) Gardea-Torresdey, J. L.; Parsons, J. G.; Gomez, E.; Peralta-Videa, J.; Troiani, H. E.; Santiago, P.; Yacaman, M. J. Formation and growth of Au nanoparticles inside live alfalfa plants. *Nano Lett.* **2002**, *4*, 397–401.

(55) Gardea-Torresdey, J. L.; Gomez, E.; Peralta-Videa, J. R.; Parsons, J. G.; Troiani, H. E.; Yacaman, M. J. Alfalfa sprouts: A natural source for the synthesis of silver nanoparticles. *Langmuir* **2003**, *19*, 1357–1361.

(56) Mukherjee, P.; Ahmad, A.; Mandal, D.; Senapati, S.; Sainkar, S. R.; Khan, M. I.; Parishcha, R.; Ajaykumar, P. V.; Alam, M.; Kumar, R.; Sastry, M. Fungus-mediated synthesis of silver nanoparticles and their immobilization in the mycelial matrix: A novel biological approach to nanoparticle synthesis. *Nano Lett.* **2001**, *1*, 515–519.

(57) Mukherjee, P.; Senapati, S.; Mandal, D.; Ahmad, A.; Khan, M. I.; Kumar, R.; Sastry, M. Extracellular synthesis of gold nanoparticles by the fungus *Fusarium oxysporum*. *Chem. Biol. Chem.* **2002**, *5*, 461–463.

(58) Southam, G.; Beveridge, T. J. The in vitro formation of placer gold by bacteria. *Geochim. Cosmochim. Acta* **1994**, *58*, 4527–4530.

(59) Greene, B.; Hosea, M.; McPherson, R.; Henzl, M.; Alexander, M. D.; Darnall, D. W. Interaction of gold(I) and gold(III) complexes with algal biomass. *Environ. Sci. Technol.* **1986**, *20*, 627–632.

(60) Battke, F.; Ernst, D.; Halbach, S. Ascorbate promotes emission of mercury vapour from plants. *Plant, Cell Environ.* **2005**, *28*, 1487–1495.

(61) Shotyk, W. Review of the inorganic geochemistry of peats and peatland waters. *Earth Sci. Rev.* **1988**, *25*, 95–176.

(62) Marcus, M. A.; MacDowell, A. A.; Celestre, R.; Manceau, A.; Miller, T.; Padmore, H. A.; Sublett, R. E. Beamline 10.3.2 at ALS: a hard X-ray microprobe for environmental and materials sciences. *J. Synchroton Radiat.* **2004**, *11*, 239–247.

(63) Proux, O.; Nassif, V.; Prat, A.; Ulrich, O.; Lahera, E.; Biquard, X.; Menthonnex, J. J.; Hazemann, J. L. Feedback system of a liquid-nitrogen-cooled double-crystal monochromator: design and performances. *J. Synchroton Radiat.* **2006**, *13*, 59–68.